



A novel non-vacuum process for the preparation of $\text{CuIn}(\text{Se},\text{S})_2$ thin-film solar cells from air-stable, eco-friendly, metal salts based solution ink



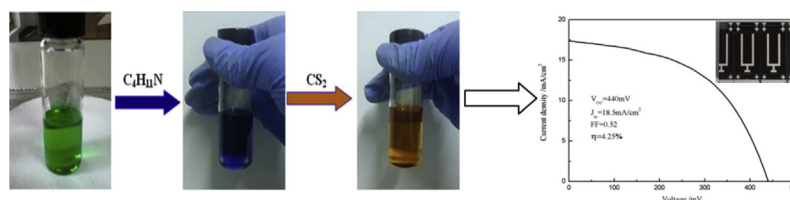
Paifeng Luo^{*}, Zhaofan Liu, Yuankui Ding, Jigui Cheng

Department of Materials Science and Engineering, Hefei University of Technology, Hefei, Anhui 230009, PR China

HIGHLIGHTS

- A simple low-cost non-vacuum process for fabrication of CISES cells was developed.
- Air-stable, low-toxic ink was successfully synthesized based on metal salts solution.
- After spin-coating and selenization process, high-quality CISES films were obtained.
- Compact chalcopyrite CISES absorber layers present superior photoelectric properties.
- The prototype PV devices with PCE of 4.25% were achieved and can be further improved.

GRAPHICAL ABSTRACT



ARTICLE INFO

Article history:

Received 22 August 2014

Received in revised form

3 October 2014

Accepted 6 October 2014

Available online 15 October 2014

Keywords:

$\text{CuIn}(\text{Se},\text{S})_2$ solar cells

Solution ink

Selenization process

Chalcopyrite

Photoelectric properties

ABSTRACT

A facile solution-based non-vacuum process for deposition of $\text{CuIn}(\text{Se},\text{S})_2$ (CISES) absorber layers is presented in this work, which indicates a promising way for the low-cost applications in thin-film solar cells. Firstly, low-boiling-point solvents Monobutylamine $\text{C}_4\text{H}_{11}\text{N}$ and Carbon disulfide CS_2 are selected as the complexing and thickening agents and added into the Cu/In metal salts based solution. Thus the air-stable, eco-friendly solution ink is successfully synthesized through a simple solution synthesis route. The detailed chemical reaction mechanism and the influence of the composition of precursor solution have been discussed intensively as well. After sequential spin-coating, hot-treatment and selenization process, the high-quality CISES films are obtained and then characterized by XRD, Raman, SEM, EDS, Metallographic microscope, Hall Effect measurement and UV–vis–NIR spectroscopy, respectively. It is found that the compact CISES films with chalcopyrite α -phase possess a double-layer structure, and also incorporate with a little ordered vacancy compounds (OVCs) and Cu_{2-x}Se impurities. The typical near stoichiometric CISES films without Carbon residuals have superior photoelectric properties with carrier concentration of $3.46 \times 10^{16} \text{ N cm}^{-3}$ and band gap of 1.15 eV. Finally, the original first-made PV devices provide a power conversion efficiency (PCE) of 4.25%, which can be further improved by increasing the thickness of CISES films and/or optimizing the selenization and sulfuration technologies.

© 2014 Elsevier B.V. All rights reserved.

1. Introduction

Currently, $\text{Cu}(\text{In,Ga})\text{Se}_2$ (CIGS) chalcopyrite thin-film solar cells are regarded as the most promising PV devices due to their high

^{*} Corresponding author. Tel.: +86 551 62904566; fax: +86 551 62905285.

E-mail address: lpfeng@hfut.edu.cn (P. Luo).

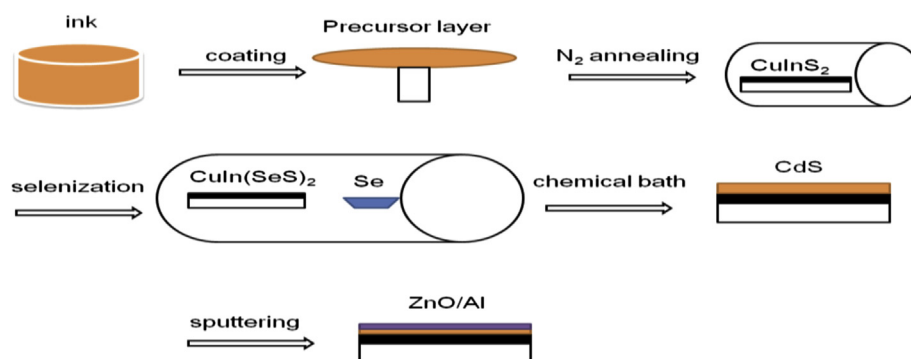


Fig. 1. The schematic diagram of the preparation of CIGS thin-film solar cells.

conversion efficiency and long term stability [1–3]. It has been demonstrated about 20% high-efficient cells by the research institutes of NREL, ZSW and EMPA using co-evaporation technology [1,4,5]. In industry, Hanergy, Solar Frontier and TSMC have been able to manufacture CIGS solar panels with efficiency above 15% employing sputtering route [5,6]. However, the vacuum-based technologies require high equipment investment and complicated production process, which seriously affect the further cost-reduction and the widespread applications in PV field. On the other hand, low-cost non-vacuum technologies showing several advantages, such as lower investment, higher material utility and easy scale-up, have been received great attentions in recent years [7–9].

Basically, non-vacuum roads can be roughly divided into two different categories: the nanoparticle or solution-based approaches. It has been widely studied using all kinds of nanoparticles as precursors, such as alloys, metal oxides and selenide quantum dots. But nanoparticles are difficult to grow up through the traditional slowly solid-phase reaction [10,11]. Meanwhile, the synthesis of the nanoparticles is always associated with fussy chemical reactions, e.g. the hot-injection and solvothermal methods. On the contrary, the easy manipulated solution-based routes can readily achieve high-quality films through fast liquid-phase reactions. Kaelin, Uhl and Yoon have prepared CIGS films by coating sticky precursor solution [12–14]. But the extra macromolecular organic additives result in a large amount of Carbon residuals in absorber layers and damage the photovoltaic properties of CIGS cells. Recently, micromolecular Hydrazine was employed as thickening agent by Mitzi and Yang with the purpose of reducing the residuals, and the highest efficiency of 15.2% in CIGS solution-based realm was achieved [15–17]. However, Hydrazine is highly toxic and explosive, and not suitable for large area applications. In this respect, more researches and development on low-toxic solution-based recipe are necessary for breakthrough in CIGS non-vacuum domain.

In this paper, a proprietary and green recipe was developed to overcome these problems. Generally, the common cheap Cu/In

metal salts are easy dissolved in ethanol solution. Low-toxic, low-boiling-point solvents Monobutylamine $C_4H_{11}N$ and Carbon disulfide CS_2 were selected as the complexing and thickening agents. $C_4H_{11}N$ has strong coordinating ability with metal cations, and can generate sticky N,N' -dibutylthiouren (DBTU) through reaction with CS_2 . Accordingly, the eco-friendly ink without micromolecular additives was readily produced by a simple solution synthesis method. Strikingly, this special solution system can be kept stably in open-air for several months. Meanwhile, Sulfur coming from CS_2 and additional sulfuration process was employed to substitute Gallium so as to adjust the band gap. Because Ga metal salts always absorb moisture in air and usually cause lattice distortion and deep-level defects in the CIGS films [18,19]. Thus comparing with CIGS absorber layers, CIGS materials have superiority in non-vacuum process. Therefore, the high-quality CIGS films were prepared by sequential spin-coating, hot-treatment and selenization process. The structure and photoelectric properties were also investigated intensively. In the end, the prototype CIGS thin-film solar cells were successfully achieved in this work.

2. Experimental

The precursor solution ink was prepared through a simple multi-step solution synthesis route. In a typical synthesis, under open-air condition, the metal salts solution with different Cu/In molar ratios was firstly synthesized by dissolving the required amount of $Cu(NO_3)_2 \cdot 3H_2O$ and $InCl_3 \cdot 4H_2O$ in ethanol with continuous stirring for 20 min. Then, $C_4H_{11}N$ and CS_2 with different dosages were used as the complexing and thickening agents. After sequentially added into the above solution and stirred for 30 min, the air-stable and viscous solution with clear yellow color was successfully obtained. All the chemicals are analytically pure grade (AR) and purchased from Sinopharm Chemical Reagent Co., Ltd. For receiving high-quality absorber layers, different molar ratio of Cu/In metal salts and the composition of the complexing agent with

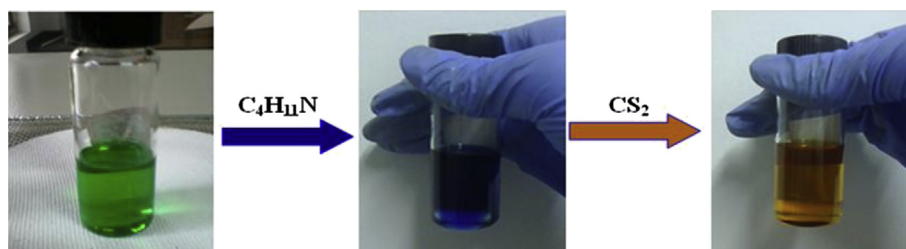


Fig. 2. The photo picture of the solution ink with different colors. (For interpretation of the references to colour in this figure legend, the reader is referred to the web version of this article.)

Table 1
Two groups of solution ink with different proportions.

Groups	Metal ions/mmol	Ethanol/mL	Monobutylamine/mL	Carbon disulfide/mL
I	5.4	6	3	1.8
II	5.4	6	6	3.6

metal ions were designed, which will be further discussed in the next part.

The synthesized ink was spin-coated on the bare glass substrate and Mo glass substrate at 2000 rpm for 30 s, respectively. After dried at 80 °C on hotplate, the same spin-coating step was repeated 5 times for thicker thickness. The hot-treatment was then processed in the quartz tube furnace under N₂ atmosphere at 350 °C for 20 min so as to remove the solvents and organics. The selenization process was performed in a two zone tubular furnace under N₂ atmosphere. The temperature of Selenium vessel was kept at 350 °C and the sample zone was heated to 550 °C and selenized for 60 min. At last, the prototype CISEs thin-film PV devices were fabricated by the traditional standard procedure. Fig. 1 shows the schematic diagram of preparation of CISEs cells. The Mo back electrode was sputtered by DC sputtering. The CdS buffer layers were deposited by chemical bath deposition (CBD). The window layers i-ZnO and AZO were prepared by RF sputtering, and the top Ni/Al electrode was evaporated by thermal evaporation.

The phase composition and the crystal structure of the films were identified by XRD method (D/Max-rA). The Raman spectra were performed in backscattering configuration at room temperature using LABRAM-HR spectrometer with 514.5 nm wavelength as a light source. The morphology of the films was observed on a field emission scanning electron microscope (FESEM, JEOL-JSM-6700F) and the metallographic microscope (LV8000). The composition of CIS films was measured by SEM-EDS. The optical absorption spectrum is recorded on a UV-vis-365-type spectrophotometer in a range of 300–1500 nm. The Hall coefficient was detected by Accent HL 5500 system. The current–voltage (*I*–*V*)

Table 2
Three groups of precursor solution with different Cu/In ratios.

Groups	Cu/In molar ratio	Ethanol/mL	Monobutylamine/mL	Carbon disulfide/mL
I	0.7	12	6	3.6
II	0.8	12	6	3.6
III	0.9	12	6	3.6

curves were measured under standard test conditions (AM1.5, TM-500D, 1000W m^{−2}, 25 °C).

3. Results and discussions

3.1. The influence of the composition of the solution ink

The proprietary recipe including the starting reagents, complexing and thickening agents employed in this work has several advantages. The common cheap metal salts Cu(NO₃)₂·3H₂O and InCl₃·4H₂O were selected as the starting reagents, which are easy dissolved in ethanol. C₄H₁₁N with low boiling point of 77.3 °C and very strong coordinating ability was used as the complexing agent. The chemical chelating reaction formulas are listed by Equations (1) and (2). At the same time, CS₂ owning lower boiling point of 46.5 °C will react with C₄H₁₁N and generate the sticky *N,N'*-dibutylthiouren (DBTU), showing by Equation (3), which can supply the suitable viscosity for following coating process and effectively solve the Carbon residuals problem. In addition, the band gap of the final absorber layer will be improved by incorporating Sulfur from the CS₂ reagent. More interestingly, the color of the solution changed immediately from green to deep blue, then to clear light yellow, as shown in Fig. 2. Surprisingly, the clear yellow solution is very stable and can be kept in air for several months, which shows the potential applied in the non-vacuum production of thin-film solar cells. All the possible reactions during the synthesis process are as following:

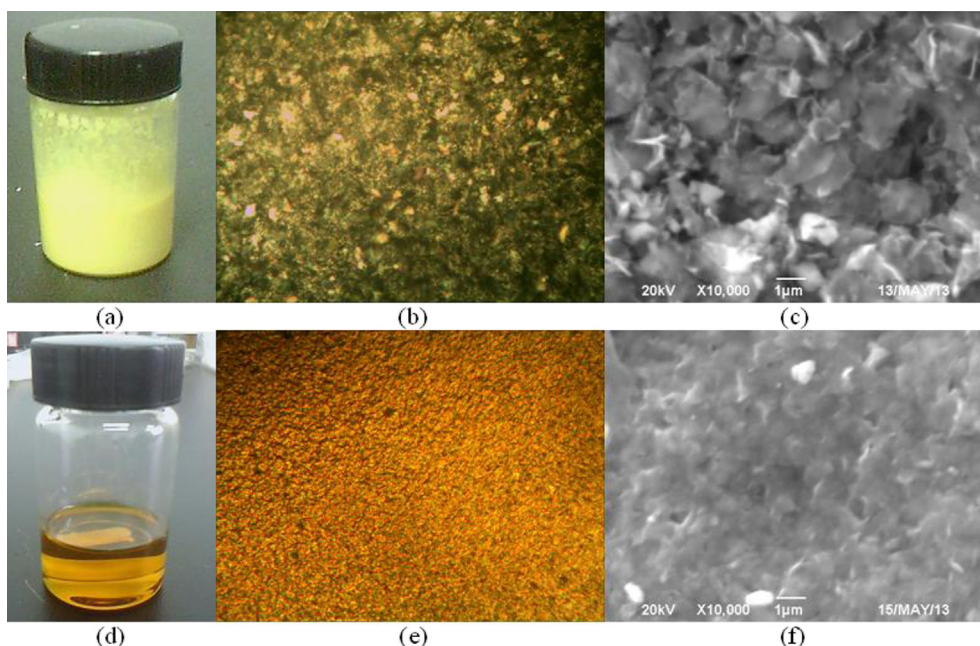
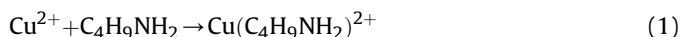


Fig. 3. The photo picture, metallurgical micrograph and the planar SEM of the two groups.

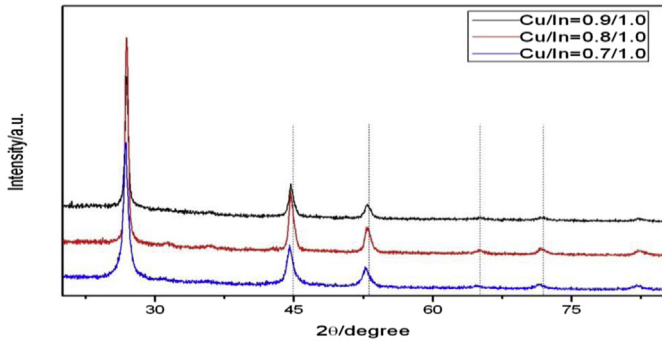
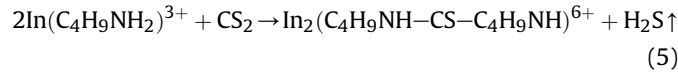
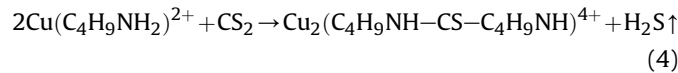
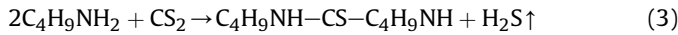
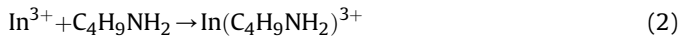


Fig. 4. The XRD patterns of CISES films of the three groups.

Table 3

The EDS of CISES films of the three groups.

Groups	Cu/At%	In/At%	Cu/In molar ratio
I	21.8	28.3	0.770
II	22.0	25.3	0.870
III	25.1	26.2	0.958



From these reaction routes, it can be deduced that the proportion of $\text{C}_4\text{H}_{11}\text{N}$ and CS_2 with metal ions is very important to obtain clear solution. To test this issue, two groups with different concentrations of $\text{C}_4\text{H}_{11}\text{N}$ and CS_2 were designed as shown in Table 1. As a result, there were a large number of nanoparticles with yellow color appeared in solution I, while the solution II were totally clear with light yellow color, as shown in Fig. 3(a) and (d), separately. The opposite phenomena were probably caused by the different amounts of complexing agent. In solution I, there was not enough $\text{C}_4\text{H}_{11}\text{N}$ to chelate the metal ions, and the rest free metal ions will react with CS_2 immediately. Fig. 3(b), (c), (e) and (f) shows

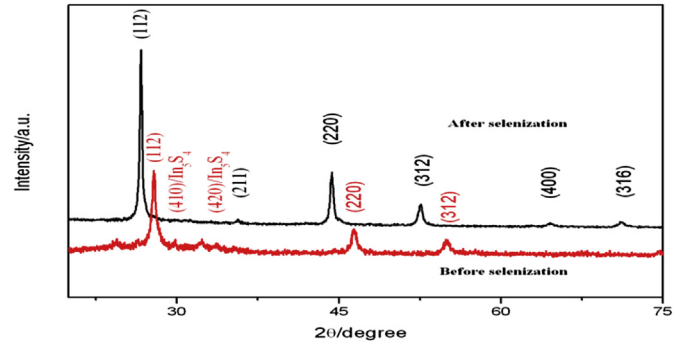


Fig. 6. The XRD patterns of CISES films before and after selenization.

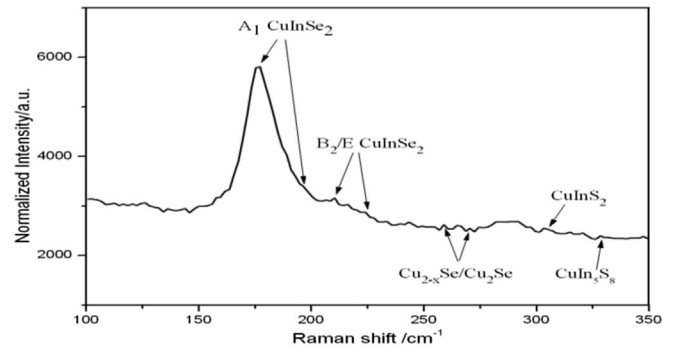


Fig. 7. The Raman spectrum of CISES films.

the metallurgical micrograph and the planar SEM of selenized CISES films on glass substrate from solution I and II, respectively. The surface of sample I is much roughness and the grain size is not uniform, while the surface of sample II is very smooth and compact. The molar content of 6 mL $\text{C}_4\text{H}_{11}\text{N}$ complexing agent is about 60 mmol in solution II. So it can be concluded that the proportion of complexing agent with metal ions should be greater than 10:1.

The molar ratio of Cu/In metal ions is also very crucial for preparing absorber layers, which will affect the conducting type and the grain size of CISES films. In this respect, three groups with Cu/In ratios of 0.7, 0.8 and 0.9 were applied to optimize the composition, as shown in Table 2. The selenized CISES films from solution I, II and III were characterized by XRD, EDS and SEM, as

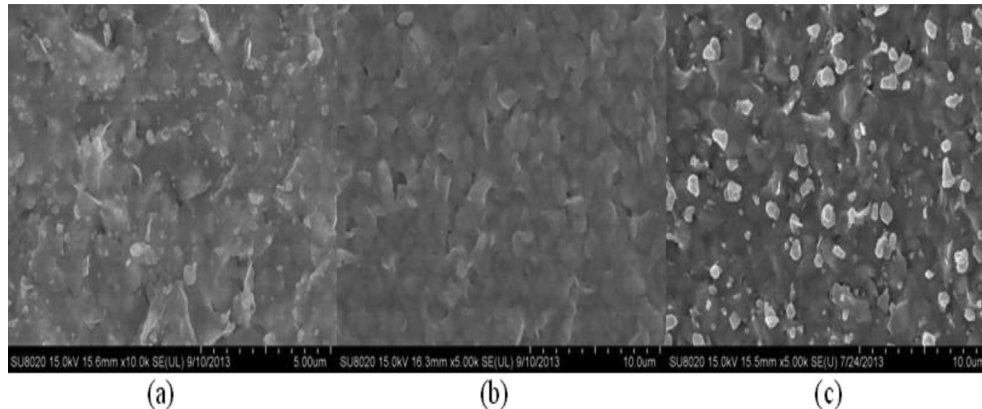


Fig. 5. The planar SEM of CISES films of the three groups.

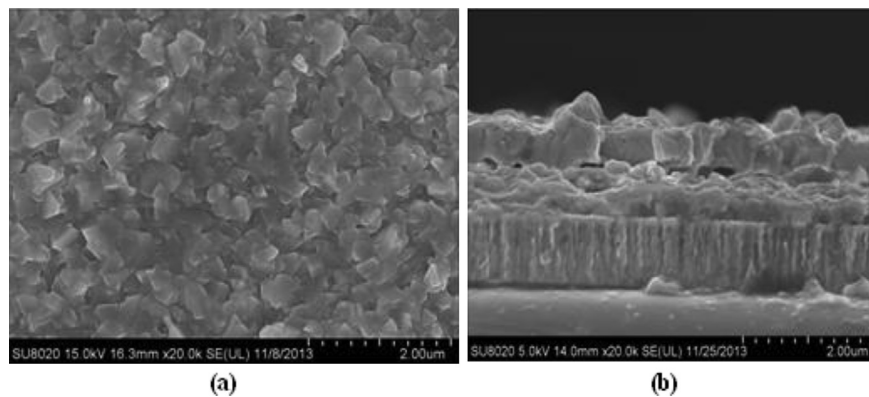


Fig. 8. The planar and cross-sectional SEM of ClSeS films.

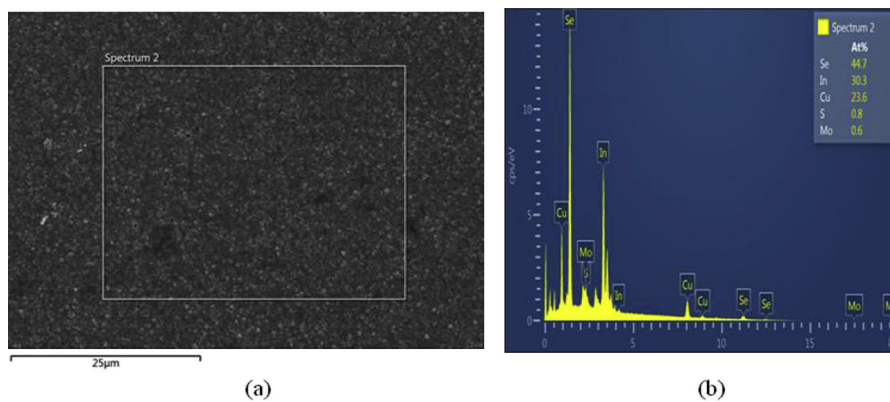


Fig. 9. The EDS of ClSeS films.

shown in Fig. 4, Table 3 and Fig. 5, separately. The results show that all the films belong to the chalcopyrite structure. The Cu/In ratios of ClSeS films are well consistent with that of the precursor solutions and only a little loss of Indium are detected. Generally, Indium can slowly react with Selenium vapor during the selenization process, thus the volatilization of the reacting product In_2Se_3 results in a small amount of Indium loss. According to our experience, the starting Cu/In ratio of 0.8 in solution II, which leads to the final ClSeS ratio of 0.870, should be the best proportion for fabrication of PV devices. The similar conclusion is

also obtained from the SEM results. There are so many small particles on the surface of Fig. 5(a) from solution I, which is caused by the In-rich composition. Meanwhile, there are a large number of big grains on the surface of Fig. 5(c) from solution III, which should be the Cu_{2-x}Se impurity phase segregated from the Cu-rich ClSeS films. Therefore, the compact and uniform ClSeS absorber layers only can be made from starting solution ratio of 0.8, as shown in Fig. 5(b). In brief, the composition of the precursor solution is a key factor for synthesizing clear ink and achieving high-quality chalcopyrite films.

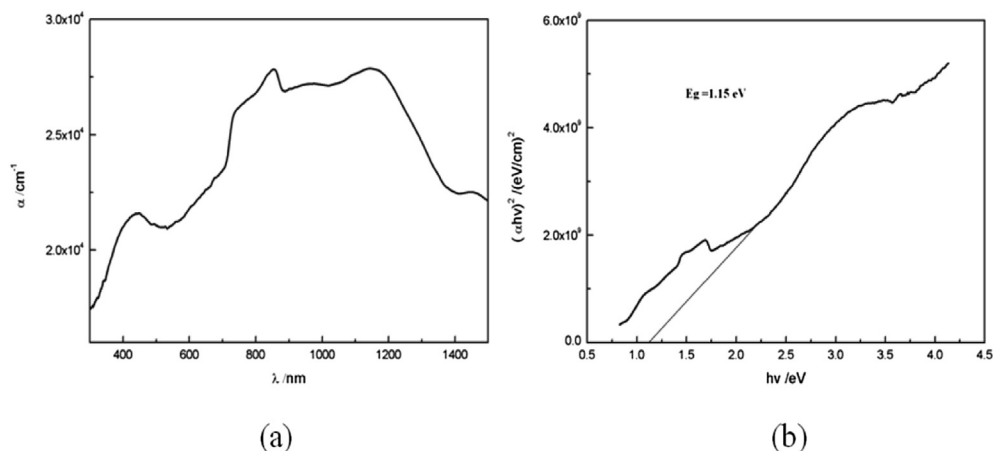


Fig. 10. (a) The wavelength dependence of the absorption coefficient and (b) the patterns of $(\alpha h\nu)^2$ against $h\nu$ of ClSeS films.

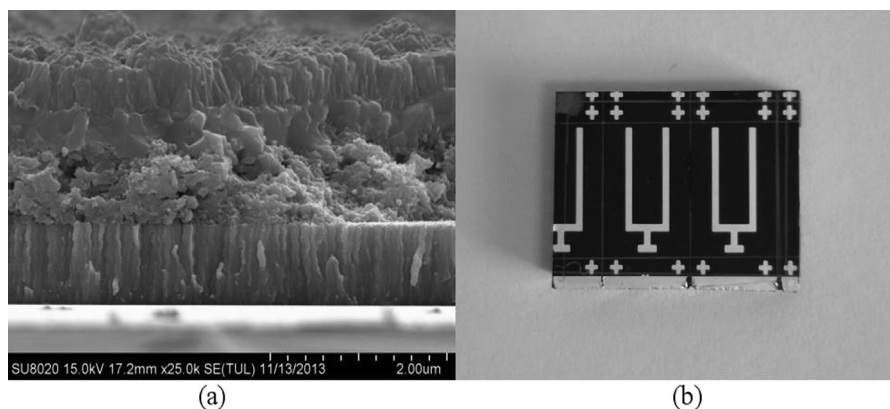


Fig. 11. The cross-sectional SEM (a) and the photo picture (b) of CISES thin-film solar cells.

3.2. The characterizations of selenized CISES films

Fig. 6 shows the X-ray diffraction patterns of CISES films before and after selenization process. Before selenization, the primary chalcopyrite phase had been formed, while the impurity phase such as In_5S_4 still existed in the precursor films. Many groups process the hot-treatment step in air [7,9,13,14], which will incorporate too much Oxygen into the CISES films and deteriorate the photovoltaic property. Therefore, herein annealing under N_2 inert atmosphere would be a better way for achieving high-quality absorber layers. After selenization, all the peaks, including the three main peaks (112), (220) and (312), belong to the chalcopyrite phase structure, and no other impurity signal can be detected from XRD patterns. The selenized CISES films have a strong preferred (112) orientation and the intensity ratio of (112) peak to (220) exceeds three times. The characteristic peaks of chalcopyrite α -CISES phase distinguishing the sphalerite δ -CISES phase, such as (211) and (400), are also detected from XRD. So the desired single chalcopyrite phase structure can be obtained through the simple non-vacuum process.

Usually, it is difficult to distinguish the chalcopyrite CIGS structure with Cu_{2-x}Se phase only through XRD investigation. In order to accurately determine the phase composition of CISES films, Raman spectra were performed using LABRAM-HR spectrometer. Fig. 7 shows the Raman spectrum of CISES absorber layers. The main A_1 mode at approximately 175 cm^{-1} and the weak B_2 and E

peaks at 217 cm^{-1} and 233 cm^{-1} always shown in chalcopyrite compounds are observed. At the same time, the weak peaks of CuInS_2 and the OVCs CuIn_5S_8 are also detected on this spectrum. The additional shoulder peak at 258 cm^{-1} different from the lattice vibrations of chalcopyrite compounds belongs to the A_1 mode of Cu_{2-x}Se phase [20]. So the detailed phase structure with some OVCs and Cu_{2-x}Se impurities in the primary CISES films is further proved by Raman spectra characterization. Additionally, OVCs and Cu_{2-x}Se impurities usually segregate on the surface of chalcopyrite films, which should be removed by diluted KCN during the process of fabrication of PV devices.

The morphology and composition of CISES films were investigated by SEM and EDS, as shown in Figs. 8 and 9, respectively. From the high-mag planar SEM as shown in Fig. 8(a), compact and well-defined CISES grains are observed after selenization process. The grain size is very uniform and attains sub-micron or micron levels. The uniformity of CISES films on a larger scale is also excellent, as shown in the low-mag EDS image of Fig. 9(a). The quality of selenized CISES films is comparable to that of preparation by traditional vacuum methods. From the cross-sectional SEM photograph in Fig. 8(b), ultrathin thickness only about $1\text{ }\mu\text{m}$ are measured, which means the spin-coating times should be increased for thicker thickness in later experiment. Apparently, the double-layer structure is also observed from the cross-sectional SEM image. The compact top layer with big grain size grows very well under adequate Selenium vapor. On the other hand, the under layer owns

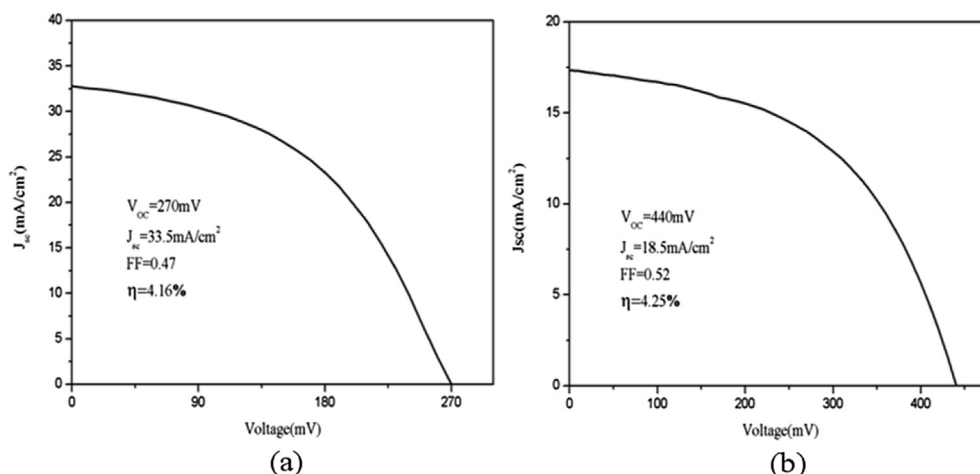


Fig. 12. The I - V curves of CISS cells (a) without sulfuration (b) with sulfuration.

the small grains with size below 0.5 μm because of the insufficient reaction dynamics. Increasing the temperature or prolonging the time of selenization process, the uniformity of CISES films will be enhanced, thus the double-layer phenomenon will be disappeared. From EDS results in Fig. 9(b), the composition of CISES films with Cu/In/(Se + S) ratio of 1/1.28/1.93 is close to the desired stoichiometry and shows a little In-rich. Apparently, no Carbon residuals have been detected, which indicates that the complexing and thickening agents are very ideal for preparing the precursor solution. Meanwhile, Sulfur is almost fully replaced by Selenium after selenization treatment. So another sulfuration step is necessary for incorporating much more Sulfur into the chalcopyrite films. In short, the typical near stoichiometric high-quality CISES absorber layers were obtained from SEM and EDS investigation.

The photoelectric properties of CISES absorber layers were characterized by Hall Effect test and UV–vis–NIR spectrophotometer, separately. The measured excellent electric properties of selenized CISES films are as following: Electric resistivity $\rho = 6 \times 10^{-2} \Omega \text{ cm}$, Hall coefficient $R_H = 1.517 \times 10^3 \text{ cm}^3 \text{ C}^{-1}$, Carrier concentration $n = 3.46 \times 10^{16} \text{ N cm}^{-3}$. Fig. 10(a) shows the wavelength dependence of the absorption coefficient of CISES films. The absorption coefficient α near $3 \times 10^4 \text{ cm}^{-1}$ was calculated by the equation $\alpha = A/0.4343d$ based on 1 μm thickness. If the thickness of CISES films increases to 2 μm , the higher absorption coefficient is expected to exceed 10^5 cm^{-1} . Meanwhile, CISES materials belong to the I–III–VI direct-gap semiconductors with valence-band maximum and conduction-band minimum at $k = 0$. According to the equation $\alpha h\nu = A(h\nu - E_g)^{1/2}$, the band gap of CISES materials can be deduced by plotting the graph between $(\alpha h\nu)^2$ vs $h\nu$. Fig. 10(b) shows the patterns of $(\alpha h\nu)^2$ against $h\nu$ for CISES absorber layers. So the band gap of 1.15 eV is received by extrapolating the straight line to $h\nu$ axis. In a word, the prepared CISES films with superior photoelectric properties are the ideal absorber layer candidate for the fabrication of solar cells.

3.3. The photovoltaic property of CISES films

The prototype CISES thin-film solar cells were assembled by sequentially deposition CdS, i-ZnO, AZO layers and evaporation of Ni/Al electrode. Fig. 11 shows the cross-sectional SEM (a) and the actual photo picture (b) of CISES devices. I – V curves of CISES cells are also shown in Fig. 12. The first-made PV devices give 4.16% PCE as shown in Fig. 12(a). The short current density J_{sc} with 33.5 mA cm^{-2} is remarkable and satisfied, but the open voltage V_{oc} and the filling factor FF are too low. The main problem would attribute to the ultrathin thickness of CISES absorber layers and the inadequate selenization technology. As mentioned in previous section, Sulfur can effectively improve the band gap of CuInSe₂ films from 1.0 eV to 1.5 eV. But almost all the Sulfur in CISES precursor films is substituted by Selenium during the selenization process, which leads to the low V_{oc} . So an additional sulfuration step was performed following the selenization process. The photovoltaic property of sulfurized CISES films was also detected and showing in Fig. 12(b). Remarkably, the V_{oc} of the sulfurized cells boosts from 270 mV to 440 mV, and the FF also has been improved. Unfortunately, the J_{sc} declines dramatically after the extra sulfuration step, and the PCE limitedly improves to 4.25%, as shown in Fig. 12(b). As a consequence, it is expected to achieve higher efficient CISES solar cells by appropriately increasing the thickness

and/or delicately optimizing the selenization and sulfuration parameters.

4. Conclusion

In conclusion, the air-stable, low-toxic solution ink was successfully developed and the low-cost non-vacuum CISES thin-film solar cells were also achieved in this study. Surprisingly, the precursor solution ink is very stable and can be kept in air for several months, which shows the potential applied in the non-vacuum production. The composition of the precursor ink was optimized and the solution synthesis mechanism was discussed as well. Meanwhile, the selenized CISES films with chalcopyrite phase structure were systematically characterized. More importantly, no Carbon residuals have been detected and the CISES absorber layers present superior photoelectric properties. In the end, near 5% conversion efficiency was obtained by the fabricated CISES PV devices, which can be further improved by optimizing the experimental parameters.

Acknowledgment

This work was financially supported by the National Natural Science Foundation of China (51302058) and the Key Project of Natural Science Foundation of the Ministry of Education of Anhui Province (KJ2011A238) and the Opening Project of CAS Key Laboratory of Materials for Energy Conversion.

References

- [1] M.A. Green, K. Emery, Y. Hishikawa, W. Wata, E.D. Dunlop, *Prog. Photovoltaics* 21 (2013) 1–11.
- [2] Y. Yan, R. Noufi, M.M. Al-Jassim, *Phys. Rev. Lett.* 96 (2006) 205501–205504.
- [3] J. Guillemoles, U. Rau, L. Kronik, H. Schock, D. Cahen, *Adv. Mater.* 11 (1999) 957–961.
- [4] A. Chirila, P. Reinhard, F. Pianezzi, P. Bloesch, A.R. Uhl, C. Fella, L. Kranz, D. Keller, C. Gretener, H. Hagendorfer, D. Jaeger, R. Erni, S. Nishiwaki, S. Buecheler, A.N. Tiwari, *Nat. Mater.* 12 (2013) 1107–1111.
- [5] P. Reinhard, S. Buecheler, A.N. Tiwari, *Sol. Energy Mater. Sol. Cells* 119 (2013) 287–290.
- [6] K. Kushiya, *Sol. Energy Mater. Sol. Cells* 122 (2014) 309–313.
- [7] C.J. Hibberd, E. Chassaing, W. Liu, D.B. Mitzi, D. Lincot, A.N. Tiwari, *Prog. Photovoltaics* 18 (2010) 434–452.
- [8] P. Luo, R. Zuo, L. Chen, *Sol. Energy Mater. Sol. Cells* 94 (2010) 1146–1151.
- [9] D. Lee, K. Yong, *Korean J. Chem. Eng.* 30 (2013) 1347–1358.
- [10] M.G. Panthani, V. Akhavan, B. Goodfellow, J.P. Schmidtke, L. Dunn, A. Dodabalapur, P.F. Barbara, B.A. Korgel, *J. Am. Chem. Soc.* 130 (2008) 16770–16777.
- [11] D.L. Schulz, C.J. Curtis, R.A. Flitton, H. Wiesner, J. Keane, R.J. Matson, K.M. Jones, P.A. Parilla, R. Noufi, D.S. Ginley, *J. Electron. Mater.* 27 (1998) 433–437.
- [12] M. Kaelin, D. Rudman, F. Kurdesau, H. Zogg, T. Meyer, A.N. Tiwari, *Thin Solid Films* 480–481 (2005) 486–490.
- [13] A.R. Uhl, C. Fella, A. Chirila, M.R. Kaelin, L. Karvonen, A. Weidenkaff, C.N. Borca, D. Grolimund, Y.E. Romanyuk, A.N. Tiwari, *Prog. Photovoltaics* 20 (2012) 526–533.
- [14] S.J. Ahn, T.H. Son, A. Cho, J. Gwak, J.H. Yun, K. Shin, S.K. Ahn, S.H. Park, K. Yoon, *ChemSusChem* 5 (2012) 1773–1777.
- [15] D.B. Mitzi, M. Yuan, W. Liu, A.J. Kellock, S.J. Chey, V. Deline, A.G. Schrott, *Adv. Mater.* 20 (2008) 3657–3662.
- [16] T.K. Todorov, O. Gunawan, T. Gokmen, D.B. Mitzi, *Prog. Photovoltaics* 21 (2013) 82–87.
- [17] B. Bob, B. Lei, C.-H. Chung, W. Yang, W.-C. Hsu, H.-S. Duan, W.W. Hou, S.-H. Li, Y. Yang, *Adv. Energy Mater.* 2 (2012) 504–522.
- [18] W. Shafarman, R. Klenk, B. McCandless, *J. Appl. Phys.* 79 (1996) 7324–7328.
- [19] U. Rau, M. Schmidt, A. Jasenek, G. Hanna, H. Schock, *Sol. Energy Mater. Sol. Cells* 67 (2001) 137–143.
- [20] W. Witte, R. Kniese, M. Powalla, *Thin Solid Films* 517 (2008) 867–869.